https://dx.doi.org/10.1016/j.proci.2022.10.004

From electronic structure to model application of key reactions for gasoline/alcohol combustion: hydrogen-atom abstraction by $CH_3O\dot{O}$ radicals

Caiyu Yang[a], Jin-Tao Chen[a], Xincheng Zhu[a], Xin Bai[e,g], Yang Li[e,g], Kiran K. Yalamanchi[f], S. Mani Sarathy[f], S. Scott Goldsborough[d], Song Cheng*[c,d], Henry J. Curran[b], Chong-Wen Zhou*[a,b]

[a]*School of Energy and Power Engineering, Beihang University, Beijing 100191, China*
[b]*Combustion Chemistry Centre, School of Chemistry, Ryan Institute, National University of Ireland, Galway, Galway H91TK33, Ireland.*
[c]*Department of Mechanical Engineering, The Hong Kong Polytechnic University, Kowloon, Hong Kong*
[d]*Energy Systems Division, Argonne National Laboratory, Lemont, IL 60439, USA*
[e]*Science and Technology on Combustion, Internal Flow and Thermostructure Laboratory, School of Astronautics, Northwestern Polytechnical University, Xi'an 710072, China*
[f]*King Abdullah University of Science and Technology (KAUST), Clean Combustion Research Center, Physical Sciences and Engineering Division, Thuwal, Saudi Arabia*
[g]*Shenzhen research Institute of Northwestern Polytechnical University, Shenzhen 518057, China*

E-mail address: songryan.cheng@polyu.edu.hk (S. Cheng), cwzhou@buaa.edu.cn (C.-W. Zhou)

Abstract

Hydrogen atom abstraction by methyl peroxy ($CH_3O\dot{O}$) radicals can play an important role in gasoline/ethanol interacting chemistry for fuels that produce high concentrations of methyl radicals. Detailed kinetic reactions for hydrogen atom abstraction by $CH_3O\dot{O}$ radicals from the components of FGF-LLNL (a gasoline surrogate) including cyclopentane, toluene, 1-hexene, *n*-heptane, and *iso*-octane have been systematically studied in this work. The M06-2X/6-311++G(d,p) level of theory was used to obtain the optimized structure and vibrational frequency for all stationary points and the low-frequency torsional modes. The 1-D hindered rotor treatment for low-frequency torsional modes was treated at M06-2X/6-31G level of theory. The UCCSD(T)-F12a/cc-pVDZ-F12 and QCISD(T)/CBS level of theory were used to calculate single point energies for all species. High pressure limiting rate constants for all hydrogen atom abstraction channels were performed using conventional transition state theory with unsymmetric tunneling corrections. Individual rate constants are reported in the temperature range from 298.15 to 2000 K. Our computed results show that the abstraction of allylic hydrogen atoms from 1-hexene is the fastest at low temperatures. When the temperature increases, the hydrogen atom abstraction reaction channel at the primary alkyl site gradually becomes dominant. Thermodynamics properties for all stable species and high-pressure limiting rate constants for each reaction pathway obtained in this work were incorporated into the latest gasoline surrogate/ethanol model to investigate the influence of the rate constants calculated here on model predicted ignition delay times.

Keywords: Hydrogen atom abstraction reaction; Methyl peroxy radical; Gasoline/ethanol interacting chemistry; Kinetic; Thermochemistry.

---

*Corresponding author.

1. Introduction

Ethanol is the main biofuel used in transportation, and its mixture with gasoline can improve anti-knock properties and reduce emissions of nitrogen oxides, carbon monoxide (CO), and particulate matter (PM). Recently, ethanol was identified by the U.S. Department of Energy Co-Optima Initiative as one of the top-10 blendstocks for modern downsized, boosted spark-ignition (SI) engines [1]. Therefore, as part of the short-term transition to low-carbon fuels, an in-depth understanding of the combustion characteristics of ethanol-blended gasoline is necessary.

Gasoline fuel is the most widely used transport fuel in the world, which consists of hundreds of hydrocarbon molecules, including alkanes, alkenes, cycloalkanes, and aromatic hydrocarbons. At present, global oil demand is doubling every year and it is expected to grow over the next 20 years, this will continue to grow according to the British Petroleum (BP) World Energy Outlook 2020 [2]. Thus, it is very important to study the characteristics of fuel combustion, to improve combustion efficiency and find surrogate fuels. Due to the complexity of their components, reduced surrogate fuels are widely used to represent real fuel components in both chemical model development and numerical simulations.

The effects of ethanol blending are complex. For example, ethanol has synergistic blending effects with octane number by blending with *n*- and *iso*-paraffins [3], and antagonistic blending effects with octane number by blending with aromatic species [4]. Therefore, it is necessary to understand the chemical interaction between ethanol and base gasoline components when predicting the mixing behavior of a surrogate fuel with ethanol when performing numerical simulations.

Recently, Sarathy et al. [5] created a 5-component gasoline surrogate, named FGF-LLNL based on the method developed at LLNL (Lawrence Livermore National Laboratory) [6], whose PIONA (paraffins, *iso*-paraffins, olefins, naphthenes, and aromatics), molar H/C ratio, and octane rating (AKI and S) are matched with the original gasoline-FACE (Fuels for Advanced Combustion Engines) gasoline. Cheng et al. [7] conducted experimental and kinetic modeling studies of FGF-LLNL autoignition, and found that discrepancies between model predictions and experimental results became larger when FGF-LLNL is blended with ethanol. Meanwhile, through sensitivity analyses of an improved gasoline surrogate model [8], Cheng et al. found that H-atom abstraction reactions by methyl peroxy ($CH_3O\dot{O}$) radicals from gasoline/alcohol surrogate components are highly important and likely responsible for the model inadequacy in replicating ethanol blending effects on FGF-LLNL.

According to Walker et al. [9], the formation and reaction of alkyl peroxy radicals, R'O$\dot{O}$ can form R'OOH *via* a H-atom abstraction reaction, which can sequentially produce more $\dot{O}H$ radicals. Curran reported that methyl peroxy ($CH_3O\dot{O}$) radical is an important abstractor at intermediate temperatures, which is crucial in the decomposition of species that generate high concentrations of methyl radicals [10]. Furthermore, $CH_3O\dot{O}$ generates CH_3OOH when it abstracts a hydrogen atom, and it subsequently decomposes to form $CH_3\dot{O}$ and $\dot{O}H$ radicals. Carstensen et al. [11, 12] used quantum chemistry to calculate rate constants for H-atom abstraction reactions from C_1~C_4 alkanes by $HO\dot{O}$, $CH_3O\dot{O}$, and $C_2H_5O\dot{O}$ radicals. However, H-atom abstraction reactions by $CH_3O\dot{O}$ radicals from larger fuel molecules have not been systematically studied.

High-level theoretical kinetic calculations of H-atom abstraction from the FGF-LLNL surrogate components including cyclopentane, toluene, 1-hexene, *n*-heptane, and *iso*-octane by $CH_3O\dot{O}$ have been performed here. The temperature-dependent thermochemical properties for all stable species have also been calculated. We have also incorporated the calculated kinetic and thermochemical data into the lasted chemistry model for FGF-LLNL/ethanol blend to investigate their influence on model performance.

2. Computational methods

The optimized geometries, vibrational frequencies, and zero-point energy (ZPE) corrections for all species and transition states were calculated based on the M06-2X method with the 6-311++G(d,p) basis set [13-15] using Gaussian 16 [16]. The intrinsic reaction coordinate (IRC) calculations were obtained in the same way. The hindrance potentials which are related to C-C, C-O, O-O single bonds were calculated at the M06-2X/6-31G level of theory and the lowest energy geometry was used as the global minima in the electronic energy calculations. The ProjRot program [17] is used to obtain the vibrational frequencies without torsional modes from the Hessian matrix calculated at the M06-2X/6-311++G(d,p) level of theory, which were then used to calculate the rate constants of the vibration partition function. The scale factors for the zero-point energies (ZPEs) were 0.9698 recommended for the M06-2X functional by Zhao et al. [13]. All possible orientations of TS for the unsymmetric molecules have been taken into consideration by defining the optical isomer of the TS. Single point energies (SPEs) for all species were performed at the UCCSD(T)-F12a/cc-pVDZ-F12 [18-20] level of theory using Molpro [21]. Additionally, Gaussian 16 [16] and ORCA [22] are also used to calculate SPEs at the QCISD(T)/CBS level of theory for comparison which can be seen in SM. QCISD(T)/CBS calculations are constructed by using the QCISD(T) energies with cc-pVDZ and cc-pVTZ basis sets and the second-order Møller–Plesset theory correction (MP2) with cc-pVDZ, cc-pVTZ, and cc-pVQZ basis sets. The SPEs were extrapolated to the complete basis set using the following equation

[23]:

$$E[QCISD(T)/CBS] = E[QCISD(T)/CBS]_{DZ\rightarrow TZ} + \{E[MP2/CBS]_{TZ\rightarrow QZ} - E[MP2/CBS]_{DZ\rightarrow TZ}\} \quad (1)$$

where

$$E[QCISD(T)/CBS]_{DZ\rightarrow TZ} = E[QCISD(T)/TZ] + \{E[QCISD(T)/TZ] - E[QCISD(T)/DZ]\} \times 0.4629 \quad (2)$$

$$E[MP2/CBS]_{TZ\rightarrow QZ} = E[MP2/QZ] + \{E[MP2/QZ] - E[MP2/TZ]\} \times 0.6938 \quad (3)$$

$$E[MP2/CBS]_{DZ\rightarrow TZ} = E[MP2/TZ] + \{E[MP2/TZ] - E[MP2/DZ]\} \times 0.4629 \quad (4)$$

The T1 diagnostics obtained at the UCCSD(T)-F12a/cc-pVDZ-F12 and QCISD(T)/aug-cc-pVTZ levels of theory for all of the species are below 0.035. Temperature-dependent rate constants for all reactions studied were calculated using conventional transition state theory with unsymmetric tunneling corrections. The rate constants were obtained in the temperature range 298.15–2000 K and were fitted to a modified Arrhenius expression of $k = A\,T^{n} \exp(-E_a/RT)$. The averaged electronic energy, obtained using the CBS-QB3 [24, 25], CBS-APNO [26], G3 [27], G4 [26] methods, was used to calculate enthalpies of formation at 0 K for all stable species based on atomization approach. Along with the 0 K formation enthalpy, the temperature-dependent partition functions for each species, calculated using MESS [18,19], were used to obtain temperature-dependent thermochemical properties including heat capacities (*C*p), enthalpies (*H*), and entropies (*S*) via the ThermP code [28]. These were finally fitted to NASA polynomial form through the PAC99 code [28, 29].

3. Result and discussion

Bond dissociation energies (BDEs) for the C–H bonds of all molecules are shown in Fig.1. It can be seen the allylic C–H bond in 1-hexene has the lowest BDE (83.67 kcal mol^{-1}), while the vinylic C–H bond in 1-hexene has the highest BDE (109.96 kcal mol^{-1}). To quantitatively analyze the effect of electron delocalization on BDEs, natural bond orbital (NBO) analyses were performed at M06-2X/6-311++G(d,p) level of theory using NBO3.1 program [30] as implemented in Gaussian 16 [16]. As can be seen, for primary C-H bonds, the value of $E^{(2)}$ ranges from 2.73 to 3.52, while the value of the BDE is 100 ± 0.35 except for the primary allylic C-H bond (88.97 kcal mol^{-1}). For secondary C-H bonds, the value of $E^{(2)}$ ranges from 5.66 to 7.74, while the value of the BDE ranged from 96.14 to 98.20 except for the secondary alkyl C-H bond in cyclopentane and for secondary allylic C-H bonds (95.13 kcal mol^{-1} and 83.67 kcal mol^{-1}, respectively). The lower BDE of the allylic hydrogen bond type in toluene and 1-hexene is due to the fact that the bond electron can delocalize to the σ*(C—H) of the allylic hydrogen bond which will weaken that bond. The ring structure helps the electron delocalization of σ*(C—H) to the adjacent σ(C—H) for C-H bond in cyclopentane.

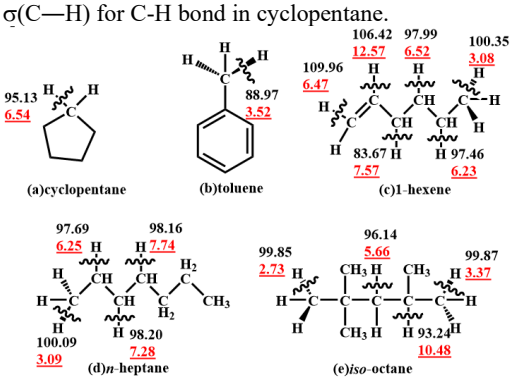

Fig.1. Second order perturbation energies $E^{(2)}$ (in red) for orbital interactions related to C-H bonds, and bond dissociation energies (in black) for the C–H bonds of the species investigated at the zero-point energy corrected UCCSD(T)-F12a/cc-pVDZ-F12//M06-2X/6-311++G(d,p) level of theory at 0 K. (Units in kcal mol^{-1}).

3.1 Electronic energy barriers

ZPE corrected energy barriers for the H-atom abstraction reactions for all channels obtained at the UCCSD(T)-F12a/cc-pVDZ-F12//M06-2X/6-311++G(d,p) levels of theory are listed in Table 1. Energy barriers calculated at the QCISD(T)/CBS level of theory using different software are similar, within an average difference of only 0.14 kcal mol^{-1}. The electronic energy barriers calculated at the UCCSD(T)-F12a/cc-pVDZ-F12//M06-2X/6-311++G(d,p) level are lower than those calculated at the QCISD(T)/CBS//M06-2X/6-311++G(d,p), level with a maximum difference of 2.46 kcal mol^{-1} and an average difference of 0.68 kcal mol^{-1}. Additionally, the electronic energy barriers calculated at the UCCSD(T)-F12a/cc-pVDZ-F12//M06-2X/6-311++G(d,p) level deviate from the average value in most cases, with a maximum difference of 1.63 kcal mol^{-1}. In general, the deviations in the calculated energy barriers from the average ones are mostly less than 1 kcal mol^{-1}. More details about the electronic energy barriers can be seen in SMM.

It should be noted that only similar sites on each molecule were discussed. Electronic energy barriers for H-atom abstraction from CH_3 groups in 1-hexene, *n*-heptane, and *iso*-octane are 19.29, 19.21, and 19.14 kcal mol^{-1} respectively, which are similar to one another. However, the barrier decreases dramatically to 14.24 kcal mol^{-1} for the abstraction of an allylic H-atom in toluene. This is consistent with the BDE calculations, as shown in Fig. 1, in which the BDE for the primary alkyl C–H bond lies 10 kcal mol^{-1} higher than the allylic C–H bond in toluene (88.97 kcal mol^{-1}). The electronic energy barrier for abstraction of a secondary alkyl H-atom in 1-hexene, *n*-heptane, and *iso*-octane is calculated to be between 15.81 ~ 16.91

kcal mol^{-1}. We also observe that the energy barrier for H-atom abstraction from cyclopentane is 15.08 kcal mol^{-1} and its BDE is at least 1 kcal mol^{-1} lower than that for the other secondary alkyl H-atom abstraction sites. In addition, the electronic energy barriers for abstraction of the allylic and vinylic H-atoms in 1-hexene are 13.42 and 24.04 kcal mol^{-1} respectively. This is consistent with the results of the BDE calculations.

Table 1
Theoretical energy barriers for H-atom abstraction reaction by $CH_3O\dot{O}$ calculated with the UCCSD(T)-F12a/cc-pVDZ-F12 level of theory using Molpro. (Unit: kcal mol^{-1}).

No.	Reaction	Forward electronic energy barrier	Reverse electronic energy barrier
R1	CPT→ c$\dot{C}_5H_9$	15.08	4.25
R2	$C_6H_5CH_3$→$C_6H_5\dot{C}H_2$	14.24	9.56
R3	C=CCCCC→$\dot{C}$=CCCCC	24.04	-0.85
R4	C=CCCCC→C=$\dot{C}$CCCC	21.07	-1.06
R5	C=CCCCC→C=C$\dot{C}$CCC	13.42	14.04
R6	C=CCCCC→C=CC$\dot{C}$CC	16.74	3.05
R7	C=CCCCC→C=CCC$\dot{C}$C	16.91	3.75
R8	C=CCCCC→C=CCCC$\dot{C}$	19.29	3.22
R9	CCCCCCC→$\dot{C}$CCCCCC	19.21	3.42
R10	CCCCCCC→C$\dot{C}$CCCCC	16.70	3.30
R11	CCCCCCC→CC$\dot{C}$CCCC	16.30	2.39
R12	CCCCCCC→CCC$\dot{C}$CCC	16.28	2.41
R13	CC(C)$_2$CC(C)C→$\dot{C}$C(C)$_2$CC(C)C	19.14	3.58
R14	CC(C)$_2$CC(C)C→CC(C)$_2\dot{C}$C(C)C	15.81	3.96
R15	CC(C)$_2$CC(C)C→CC(C)$_2$C$\dot{C}$(C)C	14.21	5.26
R16	CC(C)$_2$CC(C)C→CC(C)$_2$CC(C)$\dot{C}$	19.56	3.98

3.2 Rate constants results

The limiting high-pressure rate constants calculated on a per site basis for each system are shown in Fig. 2 in the temperature range 298.15–2000 K. Moreover, the corresponding branching ratios, calculated at the same conditions, are depicted in Fig. 3. There is little difference between the rate constants calculated using the electronic energy barriers calculated from different methods and software. The comparison of the rate constants and branching ratio obtained by using energy barriers from different computational methods is presented as SMM.

Over the entire temperature range, the rate constants for H-atom abstraction by $CH_3O\dot{O}$ from cyclopentane and the allylic site on toluene are faster compared to the other fuels due to their lower energy barriers. For the 1-hexene + $CH_3O\dot{O}$ system the rate constant for abstraction of a secondary vinylic H-atom (R3) is the slowest over the entire temperature range, while the rate constant for abstraction of an allylic H-atom (R5) is the fastest at low temperatures and is about an order of magnitude faster than that for the other channels. These are consistent with the electronic energy barriers of R3 (24.04 kcal mol^{-1}) and R5 (13.42 kcal mol^{-1}), as discussed in Section 3.1.

For the *n*-heptane + $CH_3O\dot{O}$ system the rate constants for abstraction of secondary H-atoms (R10, R11, R12) are very consistent. For these reaction channels, the maximum deviation in the energy barrier is only 0.42 kcal mol^{-1}. For the *iso*-octane + $CH_3O\dot{O}$ system the rate constant for abstraction of the tertiary alkyl H-atom (R15) is the fastest at 1000 K with the lowest energy barrier of 14.21 kcal mol^{-1}.

For each system, different H-atom abstraction reaction channels compete with each other. Figure 3(a) shows the branching ratios for H-atom abstraction by $CH_3O\dot{O}$ from 1-hexene. At temperatures above 850 K, the formation of CH_2=$CH\dot{C}H(CH_2)_2CH_3$ + CH_3OOH is gradually overcome by abstraction from the primary and secondary alkyl sites. It is worth noting that the branching ratio for abstraction of tertiary vinylic H atoms is more than 15% at temperatures above 1500 K, while H-atom abstraction from the secondary vinylic site are negligible over the entire temperature range. Figure 3(b) shows the branching ratios for the reaction between $CH_3O\dot{O}$ and *n*-heptane. The production of primary radicals, $CH_3(CH_2)_5\dot{C}H_2$ + CH_3OOH, gradually dominates with increasing temperature. Figure 3(c) shows that at T > 800 K, the production of $(CH_3)_2CHCH_2C(CH_3)_2\dot{C}H_2$ + CH_3OOH is more prevalent. The results show that the reaction of $(CH_3)_2CHCH_2C(CH_3)_3$ + $CH_3O\dot{O}$ → $(CH_3)_2\dot{C}H_2C(CH_3)_3$ + CH_3OOH is important at low temperatures and $(CH_3)_2CHCH_2C(CH_3)_3$ + $CH_3O\dot{O}$ → $(CH_3)_2CHCH_2C(CH_3)_2\dot{C}H_2$ + CH_3OOH is crucial at high temperatures.

Rate constants comparisons of different sites in the target molecules are shown in Fig. 4. The rate constant for H-atom abstraction from the terminal CH_3 group on 1-hexene is similar to that for *n*-heptane and *iso*-octane, Fig. 4(a). The rate constant for H-atom abstraction from the methylene group in cyclopentane is slightly higher than for the other secondary alkyl sites at low temperatures, Fig. 4(b). At temperatures

above 1400 K the rate constants for abstraction from alkyl CH_2 sites are within a factor of 1.9 of one another, except for cyclopentane. The rate constant for H-atom abstraction from the allylic site on 1-hexene is approximately 3.3 times higher than that from toluene over the entire temperature range.

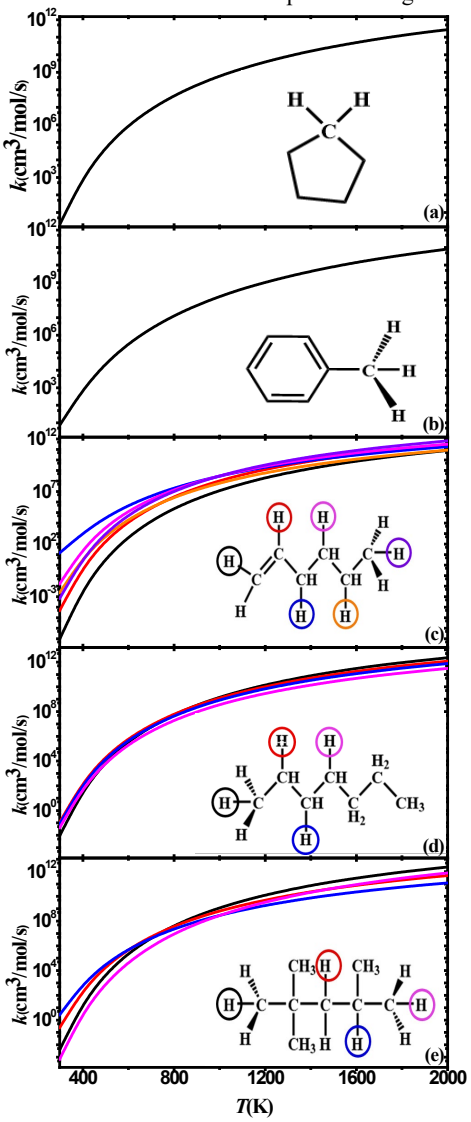

Fig. 2. Rate constants comparison for H-atom abstraction reactions on a per site basis for $CH_3O\dot{O}$ from (a) cyclopentane, (b) toluene, (c) 1-hexene, (d) *n*-heptane, (e) *iso*-octane in the temperature range 298.15–2000 K.

Rate constants comparisons between this work and NUIGMech-1.2 [31] for different reaction channels are shown in Fig. 5. Note that the rate parameters from NUIGMech-1.2 [31] were estimated by analogy. Large differences for the abstraction of primary alkyl H-atoms can be seen in Figs. 5(a) and 5(d), where the rate coefficients calculated in this study are approximately 25 and 66 times faster than those used in NUIGMech-1.2 at 2000 K for alkanes and alkenes, respectively. Figure 5(b) shows that for secondary H-atoms in alkanes the difference is within an order of magnitude over the entire temperature range. However, for cyclopentane the difference between our calculation and NUIGMech-1.2 [31] can be up to a factor of four.

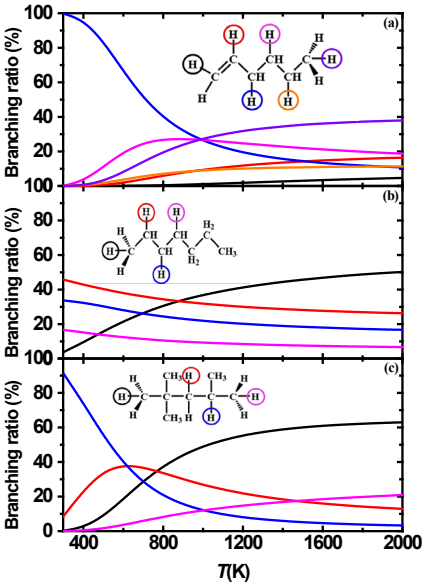

Fig. 3. Branching ratios for H-atom abstraction reactions by $CH_3O\dot{O}$ from (a) 1-hexene, (b) *n*-heptane, (c) *iso*-octane in the temperature range 298.15–2000 K.

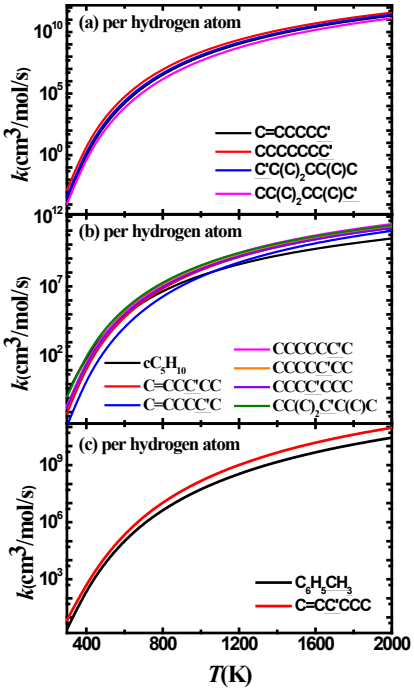

Fig. 4. Rate constants comparison for H-atom abstraction reactions on a per H-atom basis from (a) alkyl CH_3 group, (b)

alkyl CH_2 group, and (c) allylic CH_3 and CH_2 group

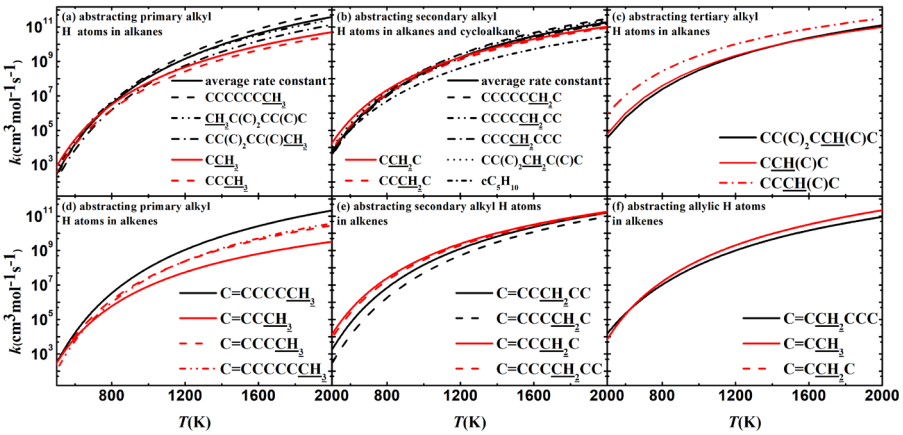

Fig. 5. Rate constants comparison for H-atom abstraction reaction on a per H-atom basis. The results of black lines represent the calculation of this work. The red lines result come from the NUIGMech 1.2 [31].

When abstracting secondary H-atoms from alkenes shown in Fig. 5(e), the ratio between this work and NUIGMech-1.2 [31] is a maximum of a factor of 50 at 500 K and this decreases to a factor of two at 2000 K. When abstracting a tertiary H-atom, it is shown in Figure 5(c) that the fastest rate constant of NUIGMech-1.2 [31] is about 26 times higher than that calculated in this work at 500 K. This ratio decreases to 2.56 at 2000 K. Figure 5(f) shows that the rate constants for abstraction of an allylic H-atom calculated here and that used in NUIGMech-1.2 [31] are within a factor of 2.5 at 500 K.

The modified Arrhenius expressions for rate constant calculations on a per site and total rate basis respectively are provided as SMM.

3.3 Thermochemical calculations

The temperature dependent thermochemical properties for all stable species were also investigated, including enthalpies of formation ($\Delta_f H^{\ominus}_{298K}$) and entropies ($S^{\ominus}_{298K}$) at 298 K. The thermochemistry data for all stable species investigated here has been compared with those in the literature including the Active Thermochemical Tables (ATcT) [32], the Third Millennium Ideal Gas and Condensed Phase Thermochemical Database for Combustion [33] (commonly called Burcat's database), the NIST Chemistry Webbook [34], and other available studies [35]. Most of the thermochemistry data calculated here agree well with the literature values. Comparisons of the thermodynamic data calculated in this work and that in the literature for all stable species and the fitted NASA polynomial coefficients are provided as SMM.

3.3 Model validation

Cheng et al. [7] measured ignition delay times (IDTs) for blends of 0 to 30% ethanol by volume with an FGF-LLNL surrogate utilizing a rapid compression machine (RCM) at pressures from 15 to 100 bar, at temperatures from 700 to 1000 K, and at equivalence ratios of 0.3 to 1.0. Blends were prepared by adding 10, 20, and 30 liquid vol. % of ethanol into neat FGF-LLNL (E0), designated as E10, E20, and E30. IDT simulations using an updated gasoline surrogate kinetic model, containing 1956 species and 10,295 reactions, were performed using the LLNL-developed fast solver Zero-RK [36] with variable volume profiles used to account for heat loss [37]. This dataset is employed herein to investigate the influence of the calculations in this work and the theory proposed in [7]. Specifically, the rate R1-R16 and the thermochemical data calculated in this work are incorporated into the chemistry model from Cheng et al [7].

The Closed Homogeneous Batch Reactor module in Chemkin is used to conduct the simulation of the RCM experiments, with the volume time histories provided by [37] to account for post-compression heat loss. The simulation results using the updated and original models along with the experiments are illustrated in Fig. 6.

It is clear that the kinetics of the reactions studied and the thermochemistry of the participating species are highly impactful, particularly for blends of ethanol and FGF-LLNL, as concluded by Cheng et al in [7]. Incorporating the updated kinetics and thermodynamic data into the model considerably increases the simulated IDTs across all temperatures with greater changes seen within the low-temperature to NTC regimes, leading to better agreement with the experimental measurements for FGF-LLNL/ethanol blends. The contribution to the reduced model reactivity by updating the thermochemistry is comparable to that by updating only the kinetics. Flux analyses are carried out for FGF-LLNL/E20 at 20%

iso-octane consumption for a stoichiometry mixture, 40 bar and 800 K using the updated model. The results are provided in Fig. S4 in SMM. The results indicate that, with the updated kinetics and thermochemistry, fluxes via H-atom abstractions by $CH_3O\dot{O}$ from the fuel molecules are enhanced, which perturb the ensuing branching pathways, eventually leading to a reduced fuel reactivity. The trends observed in Fig. 6 indicate that the kinetics and thermochemistry for these reactions and the participating species, respectively, should be included in existing chemical kinetic models, following the calculations conducted in this work.

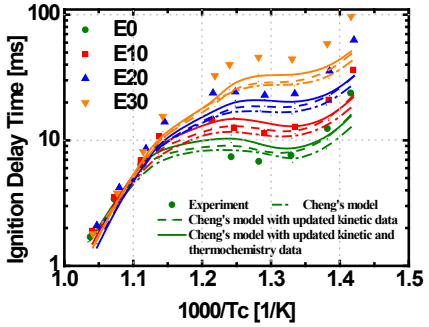

Fig. 6. Simulated and measured ignition delay time for FGF-LLNL/E0–E30 at Φ = 1.0, ~15% O_2, Pc = 40 bar and *Tc* = 700–1000 K. Simulations are conducted using the gasoline surrogate/ethanol model proposed in [7].

4. Conclusions

This work presents a systematic study of hydrogen atom abstraction by $CH_3O\dot{O}$ radicals from the components of FGF-LLNL including cyclopentane, toluene, 1-hexene, *n*-heptane and *iso*-octane. Geometry optimizations and frequency calculations of all of the species involved have been conducted at the M06-2X/6-311++G(d,p) level of theory. Electronic energies for all species were calculated at the UCCSD(T)-F12a/cc-pVDZ-F12 level of theory using Molpro and at the QCISD(T)/CBS level using Gaussian 16 and ORCA with a zero-point energy correction applied. The energy barriers for 16 reaction channels were obtained. Temperature dependent rate constants for all reaction pathways were calculated in the temperature range 298.15–2000 K, using conventional transition state theory with unsymmetric Eckart tunneling corrections. Temperature-dependent thermochemical properties for all stable species were also calculated at CBS-QB3/CBS-APNO/G3/G4 levels of theory.

The energy barriers for H-atom abstraction of secondary allylic and primary vinylic atoms from 1-hexene by CH3O$\dot{O}$ radicals are the lowest and highest respectively. Rate constants obtained by different calculation methods are within a factor of two difference. The rate constants for H-atom abstraction from the primary alkyl position of different species are consistent. At temperatures above 1200 K, rate constants for abstraction from the methylene group in cyclopentane is the lowest compared to that for 1-hexene, *n*-heptane and *iso*-octane. Over the entire temperature range, the rate constant for abstraction of a secondary allylic H-atom from 1-hexene is faster than that from toluene. Comparisons of rate constants for abstraction from similar sites (e.g., primary, secondary or tertiary alkanes) for different species obtained in this work and estimated using NUIGMech-1.2 have also been investigated systematically. Finally, the calculated kinetic and thermochemical data were incorporated into the latest gasoline surrogate/ethanol model to validate against the IDT measurements for FGF-LLNL/E0-E30 gasoline blend. The updated model is slower than the original model and is significantly more accurate compared to the experimental results in the temperature range 700–1000 K, particularly for FGF-LLNL/E30, highlighting the importance of these reactions in contributing to gasoline/ethanol interactions.

Declaration of Competing Interest

The authors declare that they have no known competing financial interests or personal relationships that could have appeared to influence the work reported in this paper.

Acknowledgments

The authors acknowledge the funding support from the National Science and Technology Major Project from China (2017-III-0004-0028). This research was supported by the high-performance computing (HPC) resources at Beihang University. The work at ANL was supported by the U.S. Department of Energy, Argonne National Laboratory LDRD program No. 2021-0344, and the Laboratory Computing Resource Center at Argonne.

Supplementary material

Supplemental material is submitted along with the manuscript.

References

[1] J.T. Farrell, R. Wagner, D. Gaspar, C. Moen, Co-Optimization of Fuels & Engines: FY18 Year in Review National Renewable Energy Lab. (NREL), Golden, CO (United States) (2019).
[2] BP p.l.c., bp Energy Outlook 2020 (2020).
[3] J. Badra, A. S. AlRamadan, S. M. Sarathy, Optimization of the octane response of gasoline/ethanol blends, *Applied Energy*. 203 (2017) 778-793.
[4] H. Yuan, Y. Yang, M. J. Brear, T. M. Foong,J. E. Anderson, Optimal octane number correlations for mixtures of toluene reference fuels (TRFs) and ethanol, *Fuel*. 188 (2017) 408-417.
[5] S. M. Sarathy, G. Kukkadapu, M. Mehl, T. Javed, A. Ahmed, N. Naser, A. Tekawade, G. Kosiba, M. AlAbbad, E.

Singh, S. Park, M. A. Rashidi, S. H. Chung, W. L. Roberts, M. A. Oehlschlaeger, C.-J. Sung, A. Farooq, Compositional effects on the ignition of FACE gasolines, *Combust. Flame*. 169 (2016) 171-193.
[6] M. Mehl, J. Y. Chen, W. J. Pitz, S. M. Sarathy, C. K. Westbrook, An Approach for Formulating Surrogates for Gasoline with Application toward a Reduced Surrogate Mechanism for CFD Engine Modeling, *Energy Fuels*. 25 (2011) 5215-5223.
[7] S. Cheng, C. Saggese, D. Kang, S. S. Goldsborough, S. W. Wagnon, G. Kukkadapu, K. Zhang, M. Mehl, W. J. Pitz, Autoignition and preliminary heat release of gasoline surrogates and their blends with ethanol at engine-relevant conditions: Experiments and comprehensive kinetic modeling, *Combust. Flame*. 228 (2021) 57-77.
[8] S. Cheng, S. Scott Goldsborough, C. Saggese, S. W. Wagnon, W. J. Pitz, New insights into fuel blending effects: Intermolecular chemical kinetic interactions affecting autoignition times and intermediate-temperature heat release, *Combust. Flame*. 233 (2021) 111559.
[9] R.W. Walker, C. Morley, M.J. Pilling (Ed.), Low-Temperature Combustion and Autoignition, Elsevier, Amsterdam. (1997) 1-124.
[10] H. J. Curran, Developing detailed chemical kinetic mechanisms for fuel combustion, *Proc. Combust. Inst.* 37 (2019) 57-81.
[11] H.-H. Carstensen, A. M. Dean, Rate constants for the abstraction reactions RO2+C2H6; R=H, CH3, and C2H5, *Proc. Combust. Inst.* 30 (2005) 995-1003.
[12] H.-H. Carstensen, A. M. Dean, O. Deutschmann, Rate constants for the H abstraction from alkanes (R–H) by R′O2 radicals: A systematic study on the impact of R and R′, *Proc. Combust. Inst.* 31 (2007) 149-157.
[13] Y. Zhao, D. G. Truhlar, The M06 suite of density functionals for main group thermochemistry, thermochemical kinetics, noncovalent interactions, excited states, and transition elements: two new functionals and systematic testing of four M06-class functionals and 12 other functionals, *Theor. Chem. Acc.* 120 (2007) 215-241.
[14] Y. Li, S. J. Klippenstein, C. W. Zhou, H. J. Curran, Theoretical Kinetics Analysis for H Atom Addition to 1,3-Butadiene and Related Reactions on the C4H7 Potential Energy Surface, *J Phys Chem A*. 121 (2017) 7433-7445.
[15] Q. D. Wang, M. M. Sun, J. H. Liang, Reaction Mechanisms and Kinetics of the Hydrogen Abstraction Reactions of C(4)(-)C(6) Alkenes with Hydroxyl Radical: A Theoretical Exploration, *Int J Mol Sci*. 20 (2019)
[16] M.J. Frisch, G.W. Trucks, H.B. Schlegel, et al., Gaussian 16 Revision C.01, (2016).
[17] C. Cavallotti, M. Pelucchi, Y. Georgievskii, S. J. Klippenstein, EStokTP: Electronic Structure to Temperature- and Pressure-Dependent Rate Constants-A Code for Automatically Predicting the Thermal Kinetics of Reactions, *J Chem Theory Comput*. 15 (2019) 1122-1145.
[18] T. B. Adler, G. Knizia, H. J. Werner, A simple and efficient CCSD(T)-F12 approximation, *J Chem Phys*. 127 (2007) 221106.
[19] G. Knizia, T. B. Adler, H. J. Werner, Simplified CCSD(T)-F12 methods: theory and benchmarks, *J Chem Phys*. 130 (2009) 054104.
[20] K. A. Peterson, T. B. Adler, H. J. Werner, Systematically convergent basis sets for explicitly correlated wavefunctions: the atoms H, He, B-Ne, and Al-Ar, *J Chem Phys*. 128 (2008) 084102.
[21] H.-J. Werner, P. J. Knowles, G. Knizia, et al., MOLPRO, version 2015.1, A Package of Ab Initio Programs.
[22] F. Neese, The ORCA program system, *Wiley Interdisciplinary Reviews: Computational Molecular Science*. 2 (2012) 73-78.
[23] P. Zhang, S. J. Klippenstein, C. K. Law, Ab initio kinetics for the decomposition of hydroxybutyl and butoxy radicals of n-butanol, *J Phys Chem A*. 117 (2013) 1890-1906.
[24] J. A. M. r, M. J. Frisch, J. W. Ochterski, G. A. Petersson, A complete basis set model chemistry. VI. Use of density functional geometries and frequencies, *J Chem Phys*. 110 (1999) 2822-2827.
[25] J. A. Montgomery, M. J. Frisch, J. W. Ochterski, G. A. Petersson, A complete basis set model chemistry. VII. Use of the minimum population localization method, *J. Chem. Phys.* 112 (2000) 6532-6542.
[26] J. W. Pchterski, G. A. Petersson, J. A. M. Jr, A complete basis set model chemistry. V. Extensions to six or more heavy atoms, *J Chem Phys*. 104 (1996) 2598-2619.
[27] L. A. Curtiss, K. Raghavachari, P. C. Redfern, V. Rassolov, J. A. Pople, Gaussian-3 (G3) theory for molecules containing first and second-row atoms, *J Chem Phys*. 109 (1998) 7764-7776.
[28] M. Keçeli, S.N. Elliott, Y.-P. Li, M.S. Johnson, C. Cavallotti, Y. Georgievskii, W.H. Green, M. Pelucchi, J.M. Wozniak, A.W. Jasper, Automated computational thermochemistry for butane oxidation: A prelude to predictive automated combustion kinetics, Proceedings of the Combustion Institute 37 (2019) 363-371.
[29] B.J. McBride, Computer program for calculating and fitting thermodynamic functions, National Aeronautics and Space Administration, Office of Management 1992.
[30] J. E. W. Carpenter, F, Analysis of the geometry of the hydroxymethyl radical by the “different hybrids for different spins” natural bond orbital procedure, *J Mol Struct (Theochem)*. 164 (1998) 41.
[31] S. Martinez, M. Baigmohammadi, V. Patel, S. Panigrahy, A. B. Sahu, S. Nagaraja, A. Ramalingam, K. A. Heufer, A. Pekalski, H. J. Curran, A comprehensive experimental and modeling study of the ignition delay time characteristics of ternary and quaternary blends of methane, ethane, ethylene, and propane over a wide range of temperature, pressure, equivalence ratio, and dilution, *Combust. Flame*. 234 (2021) 111626.
[32] B. Ruscic, D.H. Bross, Active Thermochemical Tables (ATcT) values based on ver. 1.122r of the Thermochemical Network, (2021).
[33] A. Burcat, B. Ruscic, Chemistry, T.I.I. of Tech, Third millenium ideal gas and condensed phase thermochemical database for combustion (with update from active thermochemical tables), (2005).
[34] C.E. Lemmon, M. McLinden, D. Friend, W.M. P. Linstrom, NIST Chemistry Webbook, NIST Standard Reference Database Number 69, National Institute of Standards and Technology: Gaithersburg, (2021).
[35] J. M. Simmie, K. P. Somers, Benchmarking Compound Methods (CBS-QB3, CBS-APNO, G3, G4, W1BD) against the Active Thermochemical Tables: A Litmus Test for Cost-Effective Molecular Formation Enthalpies, *J Phys Chem A*. 119 (2015) 7235-7246.
[36] M. J. McNenly, R. A. Whitesides, D. L. Flowers, Faster solvers for large kinetic mechanisms using adaptive preconditioners, *Proc. Combust. Inst.* 35 (2015) 581-587.
[37] S. Cheng, D. Kang, A. Fridlyand, S. S. Goldsborough, C. Saggese, S. Wagnon, M. J. McNenly, M. Mehl, W. J.

Pitz,D. Vuilleumier, Autoignition behavior of gasoline/ethanol blends at engine-relevant conditions, *Combust. Flame*. 216 (2020) 369-384.